Multiple low-energy excitation states in FeNi disks observed by broadband ferromagnetic resonance measurement

Y. Huo,[1] C. Zhou,[1] L. Sun,[1] S. T. Chui,[2,*] and Y. Z. Wu[1,3,†]

[1]*Department of Physics, State Key Laboratory of Surface Physics, Fudan University, Shanghai 200433, People's Republic of China*

[2]*Bartol Research Institute and Department of Physics and Astronomy, University of Delaware, Newark, Delaware 19716, USA*

[3]*Collaborative Innovation Center of Advanced Microstructures, Nanjing 210093, People's Republic of China*

(Received 21 April 2016; revised manuscript received 23 October 2016; published 17 November 2016)

Magnetization excitation in micron sized FeNi disks with different diameters is studied by broadband ferromagnetic resonance (FMR) measurement. Except the main FMR peak, additional adsorption peaks with lower energies are observed. Both micromagnetic simulation and quantum spin wave calculation confirm that the low-energy excitation states are attributed to backward volume magnetostatic (BVM) spin waves. The size dependence of the low-energy states is systematically studied in 50-nm-thick Py disks with diameters larger than 500 nm, and the linewidth of the first BVM state is found to be obviously smaller than that of the FMR absorption peak. Through a quantitative comparison with experimental results, the quantum spin wave calculation is proven to be a reliable method to get the susceptibility and is much faster than the classical micromagnetic simulations.

DOI: 10.1103/PhysRevB.94.184421

Understanding the elementary excitations in ferromagnets with finite size is very important for exploring nanomagnetism [1,2] and is also essential for designing new spintronics devices [3,4]. In nano and micron sized ferromagnets, due to the boundary condition, the quantized spin wave states can be excited in addition to the "uniform" ferromagnetic resonance (FMR) mode in the microwave frequency region [1,2,5–18]. A detailed understanding of the spectrum and the spatial wave function of quantized spin excitation is crucial for fundamental studies of magnetization dynamics. The main FMR peak corresponds to the mode(s) with the largest coupling to the external radio frequency (rf) field with the wave vector of $\mathbf{k} \sim 0$. Because of the dipolar interaction, the backward volume magnetostatic (BVM) mode with a small wave vector $\mathbf{k}$ parallel to the in-plane magnetization $\mathbf{M}$ ($\mathbf{k}//\mathbf{M}$) has lower energy than the $\mathbf{k} \sim 0$ mode. For $\mathbf{k} \perp \mathbf{M}$, both the Damon-Eshbach (DE) mode (or the magnetic surface plasmon mode) [1,2] and the regular spin wave mode are higher in energy. The DE mode has been broadly and systematically discussed [6–13]. The BVM mode is important in the fundamental understanding of nonlinear spin-wave dynamics [19,20] and applications [14,21,22], and there have been very interesting nonlinear spin wave scattering (Brillouin light scattering [BLS]) [8–10], Kerr microscopy [11], and microwave studies [12,14] on the BVM mode. Yet there has been no direct quantitative comparison between theory and experiment on the nature of the magnon wave function. The BVM mode is not easy to be observed clearly in experiments because its energy is close to that of the main FMR peak. Another spin excitation called edge mode also exists in the low-energy region besides the BVM, and this additional excitation may lead to the complexity of the spectrum [12,23]. The edge mode excitation is usually localized in the edge area of the confined magnetic structure, and recent studies [24–26] show that the edge mode will have a significant effect on the magnetization dynamics when the size of the ferromagnet is decreased to hundreds of nanometers. Thus, a detailed and systematic study of the excitation states in the low-energy region is necessary for a further understanding of magnetization dynamics in ferromagnets of finite size.

Spin wave excitations can be theoretically calculated by classical micromagnetic simulations based on the Landau-Lifshitz-Gilbert (LLG) equation [9–12,24–28], hybrid micromagnetic simulation based on dynamic matrix approaching [16,29,30], and quantum treatment through the diagonalization of the magnon Hamiltonian matrix [23]. While the spin wave excitation energies calculated via classical micromagnetic simulations or direct diagonalization of the dynamic matrix [29] are the same as those from the quantum treatment, as we explain below, the magnetic susceptibility from quantum treatment is not the same as that from a classical calculation. The susceptibility involves the expectation value of the product of two noncommuting operators. Classical calculations approximate these by the product of two commuting numbers. Micromagnetic simulation [9–12,24–28] tracks the time evolution of the average magnetization and is quite time consuming. Quantum treatment [23] can more efficiently reconstruct all the normal modes and the wave function of spin wave excitations since this method independently tracks the time evolution. Through the wave function of spin wave excitations, the frequency dependent magnetic susceptibility can be computed and compared directly with that obtained in FMR measurements, which has not been studied before.

In this paper, we studied the transmission spectrum of Py ($Ni_{80}Fe_{20}$) disks with 50-nm thickness and different diameters by the broadband FMR measured by vector network analyzer (VNA), and a set of resonance peaks were observed besides the FMR peak. By both micromagnetic simulation and quantum spin wave calculation [23], these excitation states were confirmed to be dominated by the BVM excitation. Our paper shows that the spin wave calculation by quantum treatment can enable a first-principle calculation for the frequency dependent susceptibility, in good agreement with experimental results, and is comparable in speed to classical dynamic matrix treatments but two orders faster than ordinary micromagnetic simulations. Furthermore, we find that the linewidth

*chui@bartol.udel.cn

†wuyizheng@fudan.edu.cn

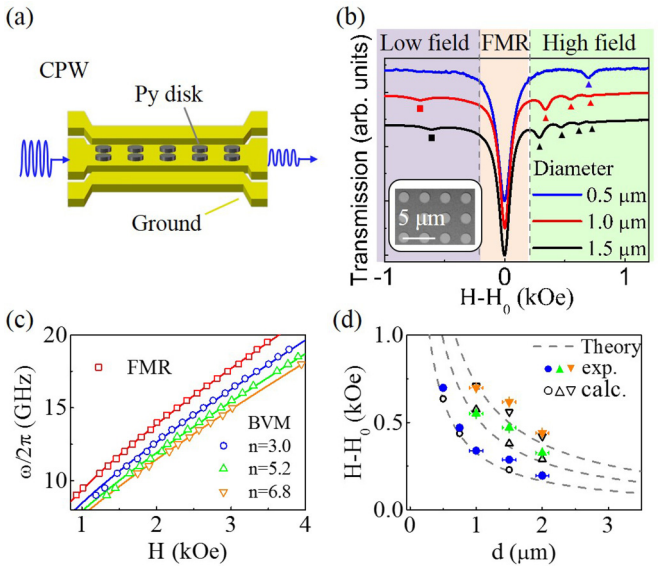

FIG. 1. (a) Sketch of sample geometry and measurement setup of the microwave transmission spectrum. (b) Typical transmission spectrums of disks with different diameters. Besides FMR, excitation states in the high field region (▲) as well as the low field region (■) were observed. The inset is a typical scanning electron microscope image of disks. (c) The ω-H dispersion of the FMR peak and the BVM modes for the disks with $d = 1\,\mu$m. The lines are the fitting curve with the Kittle formula and Eq. (1) with different excitation order n. (d) The offset field between the BVM peaks and the FMR peaks as a function of the disk size. The microwave frequency f is 14 GHz. The solid and hollow symbols are the experimental data and the calculated result by the quantum spin wave method, and the dashed lines are theoretical simulations calculated using Eq. (1) with $n = 3$, 5, and 7, respectively.

of the BVM state is obviously smaller than that of FMR absorption.

For the FMR measurement, the co-planar waveguide (CPW) was deposited on the SiO_2 substrate via magnetron sputtering of 200-nm Au; the width of the signal line is 50 μm, and the gap between the signal line and the ground is 100μ m. A 4 × 500 disk array was fabricated on the top of the signal line of the CPW by e-beam lithography and standard lift-off process. A 50-nm-thick Py ($Ni_{80}Fe_{20}$) film was deposited via e-beam evaporation. All the Py disks in each sample have the same diameter d and the same center-to-center distance D, as indicated by the inset in Fig. 1(b). We then fabricated a series of samples with different d and D. For the samples with different disk size ($d = 0.5, 0.75, 1, 1.5, 2$ μm), D is always equal to $2d$ if not specified. As discussed in Ref. [33], for D/d larger than 2, the dipole interaction between disks has very little influence on the magnetic dynamics. For the disks with $d = 1\,\mu$m, the samples with different D were fabricated to confirm the validity of ignoring the dipole interaction between disks. During the FMR measurement, the magnetic field was applied in the film plane. A constant microwave is applied through the CPW by the VNA, and the transmission spectrum is measured by sweeping the magnetic field.

Figure 1(b) shows three typical transmission spectrums of the disks with different diameters of 0.5 μm, 1 μm, and 1.5 μm; several absorption peaks can be observed in each spectrum. The strongest adsorption peak corresponds to the nearly uniform FMR peak, and the rest of the peaks are due to the spin wave excitation or the edge mode. Two kinds of spin wave modes can be excited with H applied in the plane; one is the BVM mode, and the other is the DE mode or surface mode [1,2,12]. The DE mode has higher energy than FMR and should appear in the lower field region for a given microwave frequency, while the BVM mode has lower energy and should appear in the higher field region. In our samples, the adsorption peaks in the low field region with higher energy than that of the main FMR peak are very weak, thus here we only focus on the low-energy excitation states.

Figure 1(c) shows the representative ω-H dispersions of the adsorption peaks for the disk with $d = 1\,\mu$m. The FMR dispersion follows well the Kittel Formula [31]. Through fitting, we can obtain the typical physical parameters such as the effective magnetization $M = 9.5$ kOe and the gyromagnetic ratio $\gamma = 28.9$ GHz/T of Py, and those parameters are the same as those obtained from the uniform Py film. The dispersion of low-energy states can be well approximated by the BVM dispersion for bulk spin waves. The BVM is the ordinary spin wave excitation mode with the wave vector parallel to the magnetic field, and the dispersion in a two dimensional film can be described as [2]

$$\omega^2 = \omega_0^2 + \omega_0\omega_M\left(\frac{1 - e^{-kt_F}}{kt_F}\right). \tag{1}$$

Here $\omega_0 = \gamma H$, $\omega_M = \gamma M$, t_F is the film thickness, k is the wave vector which is equal to $n\pi/w$ with n as the number of half-wave-length, and w as the confinement size. In the disk systems, w refers to the disk diameter. According to Eq. (1), due to the positive kt_F value, the energy of the BVM state should be lower than that of FMR. When $kt_F = 1$, Eq. (1) can be simplified as $\omega^2 = \omega_0^2 + \omega_0\omega_M - \omega_0\omega_M kt_F/2$. Comparing with the Kittel formula, the offset between the excitation field of BVM and the FMR field is determined by $\omega_0\omega_M kt_F/2$. The field offset between the FMR and the first BVM peak decreases with the disk size, consistent with the spectra in Fig. 1(b). According to Eq. (2), this offset field increases with the disk thickness. In our case, the disk thickness of 50 nm is thicker than that in most former studies [8–12,24–26] of the excitation in microsized systems. In our samples, the field offset between the FMR and the first BVM peak can be about 340 Oe with the microwave frequency of 14 GHz, much larger than the linewidth (~100 Oe) of FMR, which makes it possible to clearly resolve the BVM adsorption peaks, as shown in Fig. 1(b). It should be noted that the collective absorption signals of up to the fourth order of BVM modes can be observed, as shown in Fig. 1(d), and this indicates that the microdisks in our samples are very uniform with high quality. The dispersion of the lower energy peaks in Fig. 1(c) can be well fitted by Eq. (1). Using the parameters M and γ fitted from the main FMR dispersion and fixing $t_F/w = 0.05$, we can obtain $n = 3.0$ for the first BVM, $n = 5.2$ for the second BVM, and $n = 6.8$ for the third BVM. The good agreement of the fitting indicates that Eq. (1) can well approximate the low-energy excitation in the microsized disk. The fitted n is not an exact integer; this

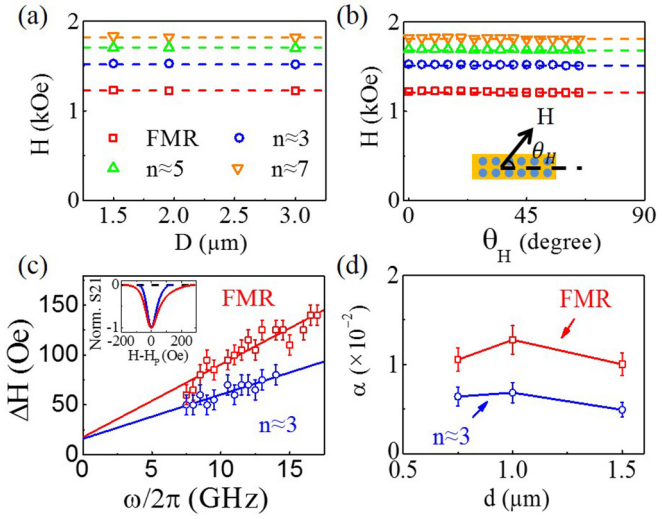

FIG. 2. (a) The dependence of excitation fields of FMR and BVM modes on (a) the core-core distance and (b) the field angle. The disk diameter is $d = 1\,\mu$m, and the microwave frequency is $f = 14$ GHz. The inset in (b) defines the field angle θ_H. (c) The FWHM of FMR and BVM as a function of the frequency for the disks with $d = 0.75\,\mu$m. The inset of (c) shows the representative normalized FMR peak and BVM peak with $n = 3$. The linewidth of the BVM mode is smaller than that of FMR. (d) The measured damping constants of the FMR peak and the BVM peak with $n = 3$ for the disks with different sizes.

is possibly attributed to the finite disk shape. w in Eq. (1) should be the effective width and may be slightly different from the diameter in the disk systems. Moreover, the edge defects in magnetic microstructures can influence the magnetization dynamics [32], which may influence the exact n value for each BVM mode. Note that the fitted n for the second and third BVM are close to the odd integer. The BVMs with the even n number are difficult to be observed in the adsorption spectrum because these states have nearly zero net magnetization and are thus weakly coupled to the uniform external driving field.

To further confirm the validity of the application of the BVM approximation, the size dependence of low-energy excitation in micro disks was systematically studied. Figure 1(d) shows the size dependence of the excitation field. The solid dots are the experimental data, and the dashed lines are calculated results for the BVM modes with $n = 3$, 5, 7, respectively. The parameters used in the calculation are from the fitting in Fig. 1(c). The experimental results follow the BVM theoretical curves very well, proving that the BVM excitation dominates the low-energy excitation observed in the micro disks.

Figure 2(a) shows the excitation fields with the fixed disk diameter $d = 1\,\mu$m and different D. The excitation fields are independent of D, indicating that the effect of long-range dipole interaction between neighboring disks is negligible for the disk with D/d larger than 2 [33]. Moreover, the excitation fields are also independent of the field angle, as shown in Fig. 2(b). The microwave excitation becomes weaker for the external field rotating toward the perpendicular direction, i.e., $\varphi_H = 90^\circ$ so that the BVM peaks can be clearly resolved only for $\varphi_H < 60^\circ$. The dipole interaction between disks should vary with the magnetization orientation. So our experiments prove that the dipole interaction between disks is negligibly small and can be ignored, thus later we discuss only the magnetization excitation of a single disk.

We found that the linewidths of the BVM peaks are clearly smaller than that of the main FMR peak. This fact can be clearly seen by the normalized BVM and FMR absorption peaks of the disk with 1 μm diameter, as shown in the inset of Fig. 2(c). Here only the first BVM and FMR excitation can be considered due to the weak signal of the higher order BVM excitation. The full width at half maximum (FWHM) ΔH can be written as $\Delta H_0 + 2\alpha\omega/\gamma$ in terms of phenomenological damping constants [34]. Here ΔH_0 is the extrinsic damping, α is the damping constant, and $\omega/2\pi$ is the microwave frequency. Figure 2(c) shows the representative frequency-dependent FWHM of both the FMR and the first BVM for the disks with $d = 0.75\,\mu$m, and both show a linear dependence. We can obtain the damping constant $\alpha = 0.01$ of FMR. This is the same as that in the Py films and also is consistent with the literature values [24,35]. By simply applying the same relation between FWHM and ω, we can obtain the damping constant $\alpha = 0.0075$ for the first BVM, which is ~25% smaller than that of FMR. Our measurement indicates that the smaller damping of BVM is an intrinsic property of the micromagnetic disk since such an effect can be found in all the disks with different diameters, as shown in Fig. 2(d).

The Gilbert damping of spin wave mode in metallic ferromagnets has also attracted great attention. The damping is usually proportional to the square of the wave number [15,36]. The damping enhancement of spin waves can be attributed to the intralayer spin current between nonuniform magnetization [37]. However, de Loubens *et al.* [27] reported a lower energy spin wave mode in a perpendicular magnetized submicron-sized Py disk, which is a localized mode at the center of film interfaces. This localized mode has lower linewidth than that of the uniform mode and was attributed to the higher k value spin wave excitation [27]. Here, for the first time, our paper points out that the BVM mode has lower damping than the uniform mode. The deduction of the BVM mode is much larger than that of the localized mode in the perpendicularly magnetized disk [27]. In fact, the BVM excitation in the square disk has also been observed with broadband FMR by Bailleul *et al.* [12], and the experimental adsorption curves inside also presented a smaller linewidth of BVM than that of FMR, which was not specifically pointed out. For a finite system with no translation symmetry, magnon states with different wave vectors but close in energy can couple to the external driving field, and all contribute to the different peaks. The slight difference in energies of these states provide an additional contribution to the widths of the peaks. Through quantum spin wave calculations described in the following, we found that more states contribute to the main peak than the BVM peaks, thus providing one source for the difference in the widths. Our results suggest further systematic studies to fully understand the mechanism of the reduced damping of BVM in the confined structures.

To identify the spatial structure of the low-energy excitation states, simulation using the program OOMMF is carried out to study the spin precession [38]. During the simulation, the parameters M, γ, and α are the fitted values from the experimental data in Fig. 1(c). We did the simulation on

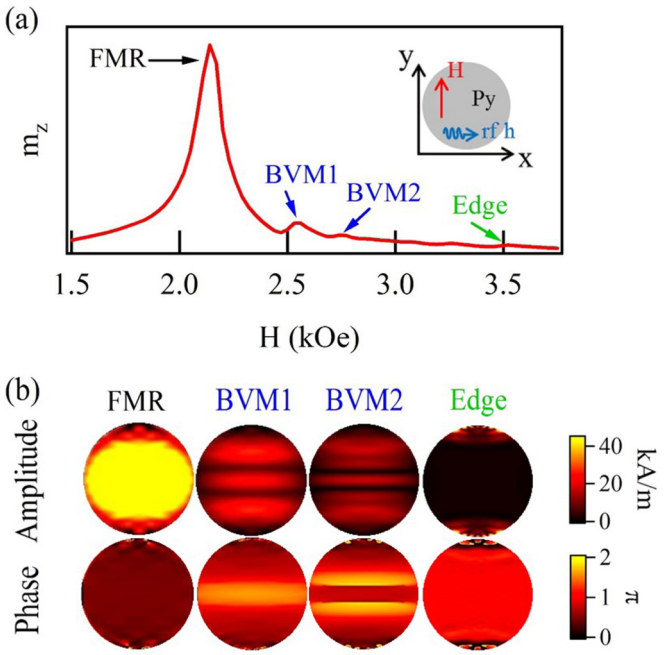

FIG. 3. Simulation results of one disk with $d = 1\,\mu$m by OOMMF excited by an rf magnetic field with $f = 14$ GHz. (a) The oscillation amplitude of dynamical magnetization m_z as a function of external field strength. (b) The spatial distribution of precession amplitude and phase of each excitation state. The inset in (a) shows the simulation geometry with the dc magnetic field applied along the y axis and the rf magnetic field along the x axis.

the disk with 50-nm thickness and 1 μm diameter. The unit cell was set as $2 \times 2 \times 50\,\text{nm}^3$. The simulation with the smaller unit cell of $2 \times 2 \times 10\,\text{nm}^3$ has been tested, which gives the same results. The microwave field **h** is applied in plane with a frequency of 14 GHz and a field amplitude of 1 Oe. The magnetic field **H** is applied in the plane but perpendicular to **h**, as shown by the inset in Fig. 3(a). By sweeping the magnetic field H, the out-of-plane magnetization precession amplitude M_z as a function of H can be calculated. Under the excitation condition, the magnetization in the disk processes with $M_z e^{-i\omega t} = \sum_j m_{zj} e^{-i(\omega t+\varphi_j)}$, here m_{zj} and φ_j are the oscillation amplitude of the out-of-plane magnetization component and the precession phase in the jth unit cell, respectively. Figure 3(a) shows the calculated M_z as a function of H. Besides the main FMR excitation, excitation in the lower field region as well as the high field region can be observed. Figure 3(b) shows the spatial distributions of the amplitude m_{zj} and phase φ_j of the spin precession in the disk. Usually the wave vector of the microwave excitation can be determined by the spatial variation of the phase φ_j. In high field excitation states, the wave vector of the spin wave aligns along the magnetic field, and this is a key character of BVM spin wave excitation [1,2]. The excitation amplitude becomes weaker for the higher excitation order n, in agreement with the experiment. In the first state, two nodes appear in the spatial phase distribution, thus the first BVM contains three half-wave lengths with $n = 3$. Besides BVM, contributions from the edge mode excitations at the two poles can, in principle, be observed; the excitation amplitude at the edge is obviously stronger for the modes in the higher field. Since the edge mode excitation is localized only in a small edge area, the total microwave adsorption should be mostly induced by the excitation inside the disk, thus the calculated mixing states should be dominated by BVM excitation.

Spin wave excitation has been theoretically studied by quantum treatment through diagonalization of the magnon Hamiltonian matrix [23]; however, this theoretical method has not been directly compared with the experimental results. Here we also performed magnon calculations with quantum treatment and compared them with the experimental results. The transmission spectrum can be determined from the susceptibility given in terms of all the magnon eigenstates by [23]

$$\chi(\omega) = i\int_{-\infty}^{t} dt' e^{i\omega(t-t')}\langle[\mathbf{S}(\mathbf{t}),\mathbf{S}(\mathbf{t}')]\rangle = \sum_j |\langle j|\mathbf{S}|0\rangle|^2/(\omega - \omega_j + i\alpha\omega). \quad (2)$$

Here $\langle j|$ indicates the jth magnon wave function, $|0\rangle$ indicates the ground state with zero field, $\hbar\omega_j$ is the energy of the jth magnon, and α is the damping constant. Here, we should emphasize that this is a quantum spin wave calculation since the susceptibility involves a *product* of two noncommuting operators, i.e., $\langle[\mathbf{S}(\mathbf{t}),\mathbf{S}(\mathbf{t}')]\rangle$, so it is not equal to the classical expression obtained by replacing the spin operators by the average value (such as by solving the classical LLG equation). For example, the normalization of the magnon wave function is determined by the commutator $[\mathbf{S}_x,\mathbf{S}_y]$ [Eq. (7) of [23]]. This condition is absent in the classical treatment. Because the quantum spin wave calculation directly addresses the elementary excitations, it is faster than the micromagnetic simulation by two orders of magnitude. This enables an efficient first-principles calculation of the frequency dependent susceptibility and the exploration of how the susceptibility depends on experimental parameters such as the disk size. We recapitulate the traditional quantum magnon calculation next.

With the method of Holstein and Primakoff [39], the magnetization operator $\mathbf{S}$ (n) for the nth spin is expressed as magnon creation and destruction operators $a(n)$, $a^*(n)$:

$$S_z(n) = (S/2)^{1/2}(a(n) + a^*(n))$$
$$S_y(n) = i(S/2)^{1/2}(a(n) + a^*(n)) \quad (3)$$
$$S_x(n) = S - a(n)a^*(n).$$

The spin wave Hamiltonian is obtained by expressing the energy of the system in terms of these operators. This Hamiltonian is then rewritten with the Bouguliubov transformation [23]. For uniform infinite size samples, the wave vector is a good quantum number, and the Hamiltonian is a 2×2 matrix, which can be easily diagonalized. For a finite system, a direct numerical diagonalization of the full spin wave Hamiltonian is carried out, as detailed in Ref. [23]. In the numerical calculation, the magnetization M was experimentally determined with 80 block spins along the diameter used, which results in more than 5100 eigenstates for the Py disk with $d = 1\,\mu$m.

Figure 4(a) shows the calculated susceptibility and the experimental adsorption spectrum with $f = 14$ GHz. In the calculation, we used the experimental value of the

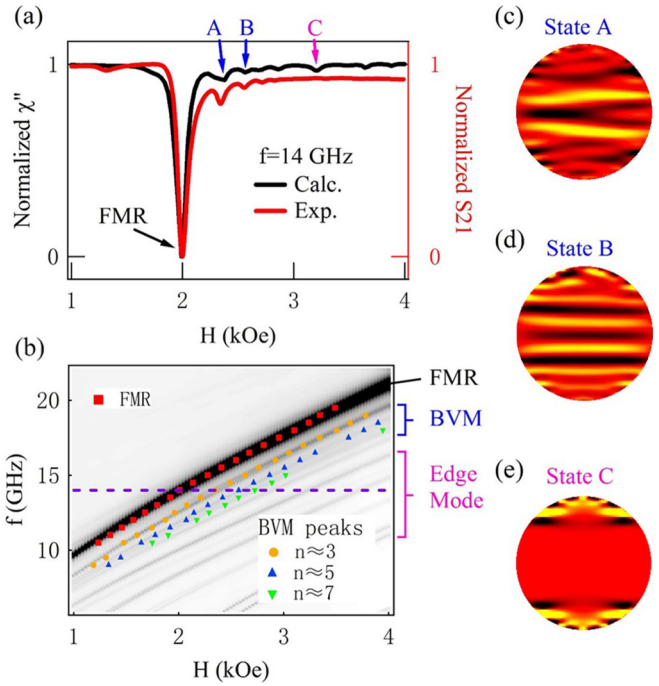

FIG. 4. Results calculated by the quantum spin wave method for the disk with $d = 1\,\mu$m. (a) Comparison of the spectra between experiment and calculation with a frequency of 14 GHz. (b) The calculated χ'' as a function of the frequency and the field. The solid dots are the experimental dispersions in Fig. 1(c)–1(e). Spatial distribution of three typical high field eigenstates A, B, and C, as marked in (b). States A and B are dominated by the BVM excitation, and state C is dominated by the edge mode.

parameters such as disk diameter of 1 μm, thickness of 50 nm, magnetization M of 9.5 kOe, and damping constant α of 0.01. The FMR peak and four high field excitation peaks were calculated with the same excitation field as the experimental results, but there are three additional excitation peaks far away from the FMR peak in the calculation. Figure 4(b) shows the calculated susceptibility as a function of f and H in the color contour. We also plot the experimental peak positions in Fig. 4(b) for comparison. The calculated results can reproduce all the observed peaks of FMR and BVM. The excitation peaks closer to the FMR peak should be dominated by the BVM mode, and this can be confirmed by the spatial distribution of the dynamical magnetization. Unlike the OOMMF output, which is the response from a driving field and is an average over the different eigenstates j given by $\sum_j \langle M_z(j)\rangle/(\omega - \omega_j + i\alpha\omega)$, Figs. 4(c) and 4(d) show the spatial distribution of the out-of-plane dynamical magnetization component of the eigenstate A and B, respectively. The spin excitation in both states spreads the entire disk plane with the wave vector perpendicular to the field with weak excitations in the edge area. Thus, the low-energy excitation states close to FMR should be the BVM mode. Figure 4(e) shows a representative dynamical magnetization distribution of the eigenstate C at $H - H_0 = 1320$ Oe, and the excited magnetization localized only at the edge(s) with the typical feature of the edge mode excitation; however, these edge mode excitations were not observed in the experiment. The edge mode is sensitive to the boundary condition of each disk; however, in reality it is difficult to have all the disk boundaries identical, thus the inhomogeneous boundaries of the disks may broaden and weaken the edge mode absorption peaks, which is in fact the integration of the adsorption of all the disks. Moreover, the size dependent excitation field in the high field region can also be calculated as the hollow indicators shown in Fig. 1(d), and the calculated results are in good agreement with the experiment. The coincidence between the calculation and the experimental results confirms that the quantum spin wave calculation can provide a direct quantitative comparison with observed absorption spectrums by first-principle calculation of susceptibility. Moreover, the quantum spin wave calculation is more efficient for reconstructing all the normal modes due to the method independently tracking the time evolution.

In summary, we systematically studied spin excitation states in the high field region with low energy in 50-nm-thick Py disks with diameters ranging from 0.5 μm to 2 μm. Both micromagnetic simulation and quantum spin wave calculation confirm that those states correspond to the BVM modes. Our results indicate that the linewidth of the BVM state is obviously smaller than that of FMR absorption. The good agreement between quantum spin wave calculations and experimental curves indicates that the quantum spin wave calculation is an efficient first-principle calculation that can be applied to analyze the absorption spectrums quantitatively. These results will help further understanding and provide new insight studying the magnetization dynamics in finite ferromagnets.

This project was supported by the National Key Basic Research Program of China (No. 2015CB921401), the National Key Research and Development Program of China (No. 2016YFA0300703) and the National Science Foundation of China (Grants No. 11434003, No. 11474066, and No. 11274074). The authors thank L. H. Bai, Y. S. Gui, and C.-M. Hu for helpful discussions. Part of the sample fabrication was conducted at Fudan Nano-fabrication Lab. S.T. Chui thanks the hospitality of the Physics Dept. of Fudan University where this paper was initiated.

[1] B. Hillebrands and K. E. Ounadjela, *Spin Dynamics in Confined Magnetic Structures* (Springer, Berlin, 2003).
[2] D. D. Stancil and A. Prabhakar, *Spin Waves: Theory and Applications* (Springer, Berlin, 2009).
[3] G. Prinz and K. Hathaway, Phys. Today **48**, 24 (1995).
[4] S. A. Wolf, D. D. Awschalom, R. A. Buhrman, J. M. Daughton, S. von Molnar, M. L. Roukes, A. Y. Chtchelkanova, and D. M. Treger, Science **294**, 1488 (2001).
[5] R. P. Erickson and D. L. Mills, Phys. Rev. B **46**, 861 (1992).
[6] J. Jorzick, S. O. Demokritov, C. Mathieu, B. Hillebrands, B. Bartenlian, C. Chappert, F. Rousseaux, and A. N. Slavin, Phys. Rev. B **60**, 15194 (1999).
[7] J. Jorzick, S. O. Demokritov, B. Hillebrands, B. Bartenlian, C. Chappert, D. Decanini, F. Rousseaux, and E. Cambril, Appl. Phys. Lett. **75**, 3859 (1999).

[8] C. Bayer, J. Jorzick, B. Hillebrands, S. O. Demokritov, R. Kouba, R. Bozinoski, A. N. Slavin, K. Y. Guslienko, D. V. Berkov, N. L. Gorn, and M. P. Kostylev, Phys. Rev. B, **72**, 064427 (2005).
[9] L. Giovannini, F. Montoncello, F. Nizzoli, G. Gubbiotti, G. Carlotti, T. Okuno, T. Shinjo, and M. Grimsditch, Phys. Rev. B **70**, 172404 (2004).
[10] F. Montoncello, L. Giovannini, F. Nizzoli, H. Tanigawa, T. Ono, G. Gubbiotti, M. Madami, S. Tacchi, and G. Carlotti, Phys. Rev. B **78**, 104421 (2008).
[11] E. R. J. Edwards, M. Buchmeier, V. E. Demidov, and S. O. Demokritov, J. Appl. Phys. **113**, 103901 (2013).
[12] M. Bailleul, R. Höllinger, and C. Fermon, Phys. Rev. B **73**, 104424 (2006).
[13] K. Vogt, O. Sukhostavets, H. Schultheiss, B. Obry, P. Pirro, A. A. Serga, T. Sebastian, J. Gonzalez, K. Y. Guslienko, and B. Hillebrands, Phys. Rev. B **84**, 174401 (2011).
[14] A. V. Chumak, A. A. Serga, B. Hillebrands, and M. P. Kostylev, Appl. Phys. Lett. **93**, 022508 (2008).
[15] Y. Li and W. E. Bailey, Phys. Rev. Lett. **116**, 117602 (2016).
[16] V. V. Naletov, G. de Loubens, G. Albuquerque, S. Borlenghi, V. Cros, G. Faini, J. Grollier, H. Hurdequint, N. Locatelli, B. Pigeau, A. N. Slavin, V. S. Tiberkevich, C. Ulysse, T. Valet, and O. Klein, Phys. Rev. B **84**, 224423 (2011).
[17] S. V. Nedukh, S. I. Tarapov, D. P. Belozorov, A. A. Kharchenko, V. O. Golub, I. V. Kilimchuk, O. Y. Salyuk, E. V. Tartakovskaya, S. A. Bunyaev, and G. N. Kakazei, J. Appl. Phys. **113**, 17B521 (2013).
[18] X. Zhou, D. Kumar, I. S. Maksymov, M. Kostylev, and A. O. Adeyeye, Phys. Rev. B **92**, 054401 (2015).
[19] A. A. Serga, B. Hillebrands, S. O. Demokritov, A. N. Slavin, P. Wierzbicki, V. Vasyuchka, O. Dzyapko, and A. Chumak, Phys. Rev. Lett. **94**, 167202 (2005).
[20] S. O. Demokritov, A. A. Serga, V. E. Demidov, B. Hillebrands, M. Kostylev, and B. A. Kalinikos, Nature (London) **426**, 159 (2003).
[21] Yu. V. Kobljanskyj, G. A. Melkov, A. A. Serga, V. S. Tiberkevich, and A. N. Slavin, Appl. Phys. Lett. **81**, 1645 (2002).
[22] M. P. Kostylev, A. A. Serga, T. Schneider, B. Leven, and B. Hillebrands, Appl. Phys. Lett. **87**, 153501 (2005).
[23] S. T. Chui, V. Novosad, and S. D. Bader, Phys. Rev. B **80**, 054419 (2009).
[24] J. M. Shaw, T. J. Silva, M. L. Schneider, and R. D. McMichael, Phys. Rev. B **79**, 184404 (2009).
[25] H. T. Nembach, J. M. Shaw, T. J. Silva, W. L. Johnson, S. A. Kim, R. D. McMichael, and P. Kabos, Phys. Rev. B **83**, 094427 (2011).
[26] F. Guo, L. M. Belova, and R. D. McMichael, Phys. Rev. Lett. **110**, 017601 (2013).
[27] G. de Loubens, V. V. Naletov, O. Klein, J. B. Youssef, F. Boust, and N. Vukadinovic, Phy. Rev. Lett. **98**, 127601 (2007).
[28] V. Novosad, M. Grimsditch, K. Yu. Guslienko, P. Vavassori, Y. Otani, and S. D. Bader, Phys. Rev. B **66**, 052407 (2002).
[29] M. Grimsditch, L. Giovannini, F. Montoncello, F. Nizzoli, G. K. Leaf, and H. G. Kaper, Phys. Rev. B **70**, 054409 (2004).
[30] M. d'Aquino, C. Serpico, G. Miano, and C. Forestiere, J. Comput. Phys. **228**, 6130 (2009).
[31] Ch. Kittel, Phys. Rev. **73**, 155 (1948).
[32] V. Flovik, F. Macià, J. M. Hernàndez, R. Bručas, M. Hanson, and E. Wahlström, Phys. Rev. B, **92**, 104406 (2015).
[33] A. Vogel, A. Drews, T. Kamionka, M. Bolte, and G. Meier, Phys. Rev. Lett. **105**, 037201 (2010).
[34] E. Montoya, T. McKinnon, A. Zamani, E. Girt, and B. Heinrich, J. Magn. Magn. Mater. **356**, 12 (2014).
[35] G. M. Sandler, H. N. Bertram, T. J. Silva, and T. M. Crawford, J. Appl. Phys. **85**, 5080 (1999).
[36] C. E. Patton and W. Jantzb, J. Appl. Phys. **50**, 7082 (1979).
[37] S. Zhang and S. S.-L. Zhang, Phys. Rev. Lett. **102**, 086601 (2009).
[38] M. Donahue and D. G. Porter, *OOMMF User's Guide*, Version 1.0, Interagency Report NISTIR 6376 (NIST, Gaithersburg, Maryland, USA, 1999).
[39] See, for example, C. Kittel, *Quantum Theory of Solids* (J. Wiley, New York, 1963).